Journal of Thermal Analysis and Calorimetry, Vol. 97 (2009) 2, 409–414

INFLUENCE OF THE SPECIFIC SURFACE AREA ON CRYSTALLIZATION PROCESS KINETICS OF SOME SILICA GELS

C. Păcurariu[1*], *R. I. Lazău*[1], *I. Lazău*[1], *R. Ianoş*[1] *and T. Vlase*[2]

[1]Politehnica University of Timişoara, P-ta. Victoriei No. 2, Timişoara 300006, Romania
[2]West University of Timişoara, Department of Chemistry, Blvd. V. Pârvan No. 4, Timişoara 300223, Romania

The influence of the specific surface area on the crystallization processes of two silica gels with different specific surface areas has been investigated in non-isothermal conditions using DTA technique. The activation energies of the crystallization processes were calculated using four isoconversional methods: Ozawa–Flynn–Wall, Kissinger–Akahira–Sunose, Starink and Tang. It has been established that, the decrease of the surface area from S=252.62 $m^2\ g^{-1}$, in the case of sample GS2, to S=2.52 $m^2\ g^{-1}$, in the case of sample GS1, has determined a slight increase of the activation energy of the crystallization process of the gels. Regardless of the isoconversional method used, the activation energy (E_α) decreases monotonously with the crystallized fraction (α), which confirms the complex mechanism of gels crystallization. It has been proved that the Johnson–Mehl–Avrami model cannot be applied for the crystallization processes of the studied silica gels.

Keywords: *crystallization kinetics, non-isothermal kinetics, silica gels*

Introduction

It is well known that the thermal treatment of silica gels leads to their crystallization, with cristobalite formation. The study of the silica gels crystallization process presents a special interest due to the temperature range (1000–1200°C), in which the cristobalite formation takes place. This is much below the temperature indicated for α-cristobalite formation (1470°C), according to Fenner's diagram [1, 2]:

$$\beta\text{-quartz} \xleftrightarrow{573^\circ C} \alpha\text{-quartz} \xleftrightarrow{870^\circ C} \alpha\text{-tridymite} \xleftrightarrow{1470^\circ C} \alpha\text{-cristobalite (high cristobalite)}$$

During the cooling process, α-cristobalite remains as a meta-stable phase until it transforms into β-cristobalite, which takes place in a temperature range between 270 and 180°C:

$$\alpha\text{-cristobalite (high cristobalite)} \xleftrightarrow{270\ldots180^\circ C} \beta\text{-cristobalite (low cristobalite)}$$

The formation of α-cristobalite at temperatures between 1000–1200°C, when α-tridymite is stable according to Fenner's diagram, is questioning the very existence of this polymorphous modification. The literature data mention that tridymite only forms from SiO_2 impurified with certain oxides (especially alkaline oxides), meaning that tridymite is a solid solution derived from SiO_2 rather than pure SiO_2.

Our studies confirmed that the thermal treatment of the considered SiO_2 gel leads directly to cristobalite.

The purpose of this work was to investigate the influence of the specific surface area on crystallization processes of two silica gels with different surface area (GS1 with surface area S=2.52 $m^2\ g^{-1}$ and GS2 with surface area S=252.62 $m^2\ g^{-1}$). Also, the crystallization mechanism of the silica gels was analyzed.

Experimental

Samples preparation

The used gel was a commercial 'Aerosil'-type gel obtained by $SiCl_4$ hydrolysis in oxyhydric flame. After thermal treatment of the mentioned gel, at temperatures of 900 and 700°C, respectively for 1 h, two gels GS1 and GS2 resulted. The two temperatures are below the crystallization temperature of such gels, but the increases from 700 to 900°C caused a 100 times decrease of the surface area, thus, of the superficial energy.

Characterization methods

For the specific surface area assessment, it has been used the BET method, with nitrogen adsorption, on a Micromeritics ASAP 2020 equipment.

* Author for correspondence: cornelia.pacurariu@chim.upt.ro

1388–6150/$20.00

Akadémiai Kiadó, Budapest, Hungary
Springer, Dordrecht, The Netherlands

The nature of the crystalline phase formed after the thermal treatment of the silica gel has been monitored by X-ray diffraction, using a DRON 3 diffractometer, MoK_α radiation.

For the kinetic studies, a series of differential thermal analysis (DTA) under non-isothermal conditions were carried out for various heating rates.

The differential thermal curves (DTA) were recorded using a Netzsch STA 449C instrument in the temperature range 30–1250°C at various heating rates: 6, 10, 14, 18, 22 K min^{-1}, using alumina crucibles.

Kinetic studies

In order to pursue the influence of the surface area on the kinetics of the crystallization process, it has been calculated the activation energy of the crystallization process of the two gels GS1 and GS2. With this view, four isoconversional methods have been used: Ozawa–Flynn–Wall (OFW), Kissinger–Akahira–Sunose (KAS), Starink and Tang. All of these methods can be represented by the general equation [3–5]:

$$\ln\frac{\beta}{T_\alpha^\kappa}=-A\frac{E_\alpha}{RT_\alpha}+C \qquad (1)$$

where κ is a constant depending on the approximation of the temperature integral employed, A and C are constants and the subscript α designates values related to a given conversion degree.

For κ=0, the Ozawa–Flynn–Wall (OFW) equation results [6–9]:

$$\ln\beta=-1.052\frac{E_\alpha}{RT_\alpha}+C \qquad (2)$$

For κ=2, results the Kissinger–Akahira–Sunose (KAS) Eq. (3) [3, 8–11]:

$$\ln\frac{\beta}{T_\alpha^2}=-\frac{E_\alpha}{RT_\alpha}+C \qquad (3)$$

For κ=1.92, results the Starink Eq. (4) [3, 8, 12]:

$$\ln\frac{\beta}{T_\alpha^{1.92}}=-1.0008\frac{E_\alpha}{RT_\alpha}+C \qquad (4)$$

For κ=1.894661, results the Tang Eq. (5) [13, 14]:

$$\ln\frac{\beta}{T_\alpha^{1.894661}}=-1.00145033\frac{E_\alpha}{RT_\alpha}+C \qquad (5)$$

For obtaining the kinetic parameters, all of these isoconversional methods involve the plotting of the left-hand side of Eqs (2)–(5) *vs.* $1/T_\alpha$.

The crystallized fraction was determined from the DTA curves using Eq. (6):

$$\alpha(T)=\frac{A_T}{A_{total}} \qquad (6)$$

where $\alpha(T)$ is the crystallized fraction at the temperature T, A_T the area at the temperature interval ΔT and A_{total} the total area of the crystallization peak.

In order to obtain information about the silica gels crystallization mechanism, the Avrami exponent n [15, 16] was calculated using the Ozawa method [17–19].

At a given temperature, the equation proposed by Ozawa [18] is expressed as:

$$\log[-\ln(1-\alpha)]=\log\chi(T)-n\log\beta \qquad (7)$$

where $\chi(T)$ is a constant.

The Avrami exponent n results from the slope of the plot of $\log[-\ln(1-\alpha)]$ as a function of $\log\beta$ at a given temperature.

Results and discussion

The specific surface area for the sample GS1, resulted by annealing the initial gel at 900°C, was S=2.52 $m^2\ g^{-1}$ and for the sample GS2, resulted by annealing the initial gel at 700°C, was S=252.62 $m^2\ g^{-1}$.

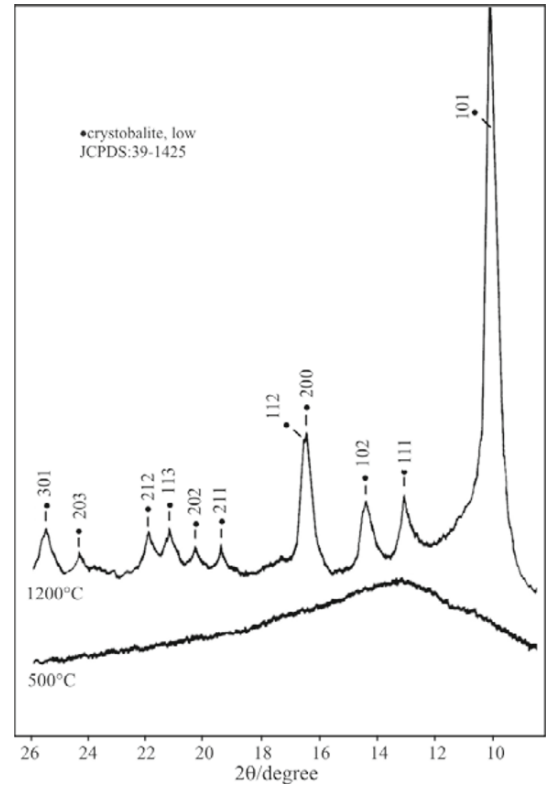

Fig. 1 XRD patterns of the silica gel annealed at 500 and at 1200°C

The silica gel's crystallization to cristobalite was confirmed by the results of the X-ray diffraction analysis. The X-ray powder diffraction patterns of the initial silica gel annealed at 500 and at 1200°C are presented in Fig. 1, showing that the silica gel annealed at 500°C is amorphous, whilst at 1200°C cristobalite appears.

The DTA curves of the sample GS2 recorded at various heating rates are shown in Fig. 2.

The temperatures at the maximum crystallization rate (temperatures of DTA peaks) of sample GS1 for different heating rates are presented in Table 1.

The dependences of the crystallized fraction α (determined from the DTA curves using Eq. (6)) on temperature for sample GS2 are presented for different heating rates in Fig. 3.

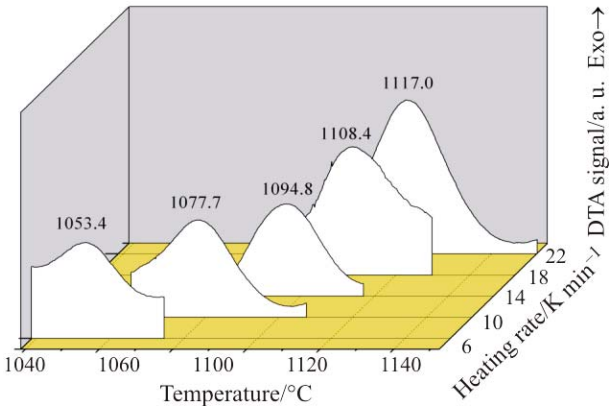

Fig. 2 DTA crystallization curves of the sample GS2 for different heating rates

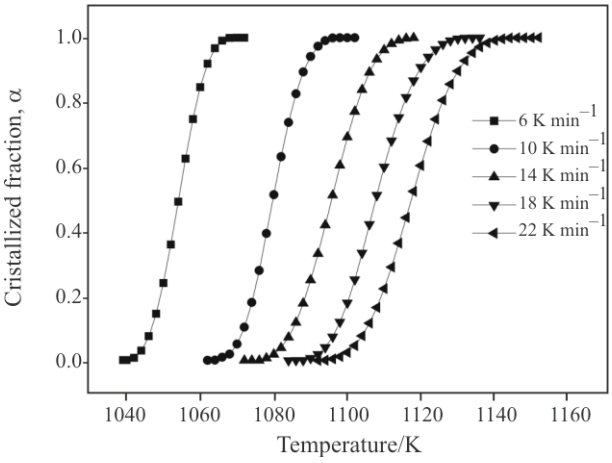

Fig. 3 Crystallized fraction α *vs.* temperature in the case of sample GS2, at different heating rates

Ozawa–Flynn–Wall method

The activation energies of the crystallization processes were estimated by using the OFW method. For constant crystallized fraction, the value of E_α was calculated from the slope of the linear fitted function of lnβ *vs.* T_α^{-1} (Eq. (2)). The OFW plots are presented in Fig. 4 for the sample GS1.

Kissinger–Akahira–Sunose method

Using the Kissinger–Akahira–Sunose method, the activation energies for the crystallization processes were calculated from the slope of the linear fitted function of $\ln(\beta/T_\alpha^2)$ *vs.* T_α^{-1} (Eq. (3)), for several crys-

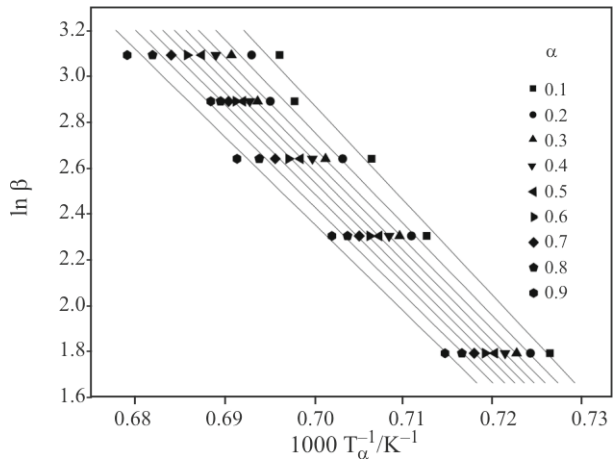

Fig. 4 Plots of lnβ *vs.* T_α^{-1} for sample GS1 at different crystallized fractions

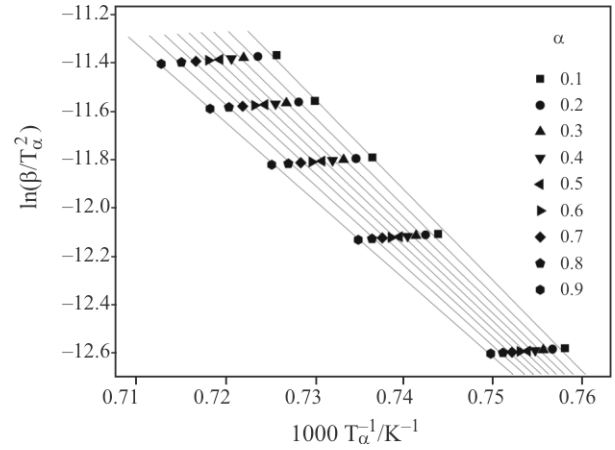

Fig. 5 Plots of $\ln(\beta/T_\alpha^2)$ *vs.* T_α^{-1} for sample GS2 at different crystallized fractions

Table 1 Temperatures of DTA peaks for different heating rates of sample GS1

Heating rate/ K min^{-1}	6	10	14	18	22
Temperatures of DTA peaks/°C	1115.5	1140.2	1158.4	1173.1	1181.2

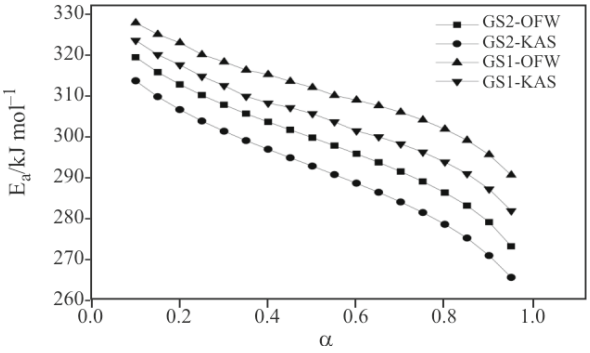

Fig. 6 Variation of E_α, calculated with the KAS and OFW methods, with α for samples GS1 and GS2

tallized fractions. The KAS plots are presented in Fig. 5 for sample GS2.

The variation of E_α, calculated with the KAS and OFW methods, with the crystallized fraction α, for the samples GS1 and GS2 is presented comparatively in Fig. 6.

As it results from Fig. 6, the activation energies values of the sample GS2 (with specific surface area S=252.62 m^2 g^{-1}) are smaller than the values of the sample GS1 (with specific surface area S=2.52 m^2 g^{-1}).

The activation energies values calculated using the KAS and OFW methods monotonously decrease with the crystallized fraction for both samples.

For both samples, GS1 and GS2, it may be observed that the E_α values calculated with KAS method are slightly lower than those calculated with OFW method.

Starink method

Using the Starink method, the value of E_α was calculated from the slope of the linear fitted function of $\ln(\beta/T_\alpha^{1.92})$ *vs.* T_α^{-1} (Eq. (4)) for constant crystallized fraction. The Starink plots for different crystallized fractions are presented in Fig. 7 for the sample GS1.

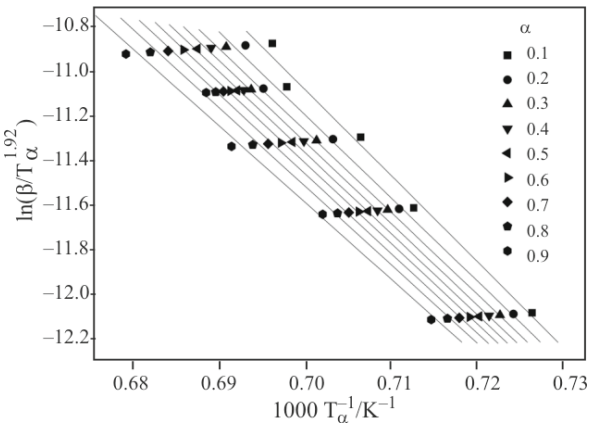

Fig. 7 Plots of $\ln(\beta/T_\alpha^{1.92})$ *vs.* T_α^{-1} for the sample GS1 at different crystallized fractions

Tang method

The activation energies for the crystallization processes were calculated from the slope of the linear fitted function of $\ln(\beta/T_\alpha^{1.894661})$ *vs.* T_α^{-1} (Eq. (5)), for several crystallized fractions. The Tang plots for different crystallized fractions are presented in Fig. 8 for the sample GS2.

The values of the activation energies for the samples GS1 and GS2, calculated with the Starink and Tang method for several crystallized fractions are shown in Table 2.

Correlating the activation energies values obtained with the four presented isoconversional methods, it may be noticed:

- The slightly lower E_α values for the sample GS2 (with specific surface area S=252.62 m^2 g^{-1}) than the values for sample GS1 (with specific surface area S=2.52 m^2 g^{-1}). Therefore, a 100 times decreases of the surface area only results in a slight activation energy increase.
- For both samples, the values for the activation energy calculated with Starink and Tang equations are very close. These values are a little lower than those obtained with the KAS and OFW method. Making a comparison, between the accuracy of the OFW, KAS and Starink methods, Starink [8] has demonstrated that the OFW method is quite inaccurate (with deviation in activation energy higher than 10%), succeeded by the KAS method (with deviation in activation energy limited to about 1%). According to Starink, the best accuracy presents the Starink method. Therefore, the E_α values obtained with Starink and Tang equations are the most accurate.
- The activation energies values decrease monotonously with the crystallized fraction for both samples no matter which isoconversional method was

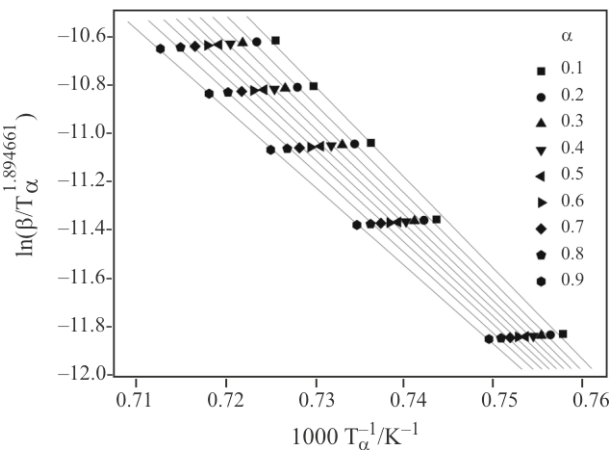

Fig. 8 Plots of $\ln(\beta/T_\alpha^{1.894661})$ *vs.* T_α^{-1} for sample GS2, at different crystallized fractions

Table 2 The activation energies and the correlation coefficients for the samples GS1 and GS2, calculated with the Starink and Tang method

α	GS1				GS2			
	Starink method		Tang method		Starink method		Tang method	
	E_a/ kJ mol^{-1}	r^2	E_a/ kJ mol^{-1}	r^2	E_a/ kJ mol^{-1}	r^2	E_a/ kJ mol^{-1}	r^2
0.1	324.39	0.9934	324.59	0.9934	314.41	0.9987	314.49	0.9986
0.2	318.17	0.9965	318.30	0.9966	307.32	0.9991	307.41	0.9991
0.3	313.07	0.9979	313.27	0.9980	302.03	0.9994	302.11	0.9995
0.4	308.70	0.9993	308.90	0.9993	297.57	0.9995	297.66	0.9995
0.5	305.89	0.9999	306.19	0.9999	293.44	0.9996	293.53	0.9996
0.6	302.14	0.9998	302.24	0.9998	289.24	0.9997	289.34	0.9998
0.7	298.76	0.9991	298.83	0.9991	284.62	0.9997	284.72	0.9997
0.8	294.01	0.9977	294.11	0.9970	279.12	0.9998	279.22	0.9998
0.9	287.85	0.9918	287.95	0.9918	271.44	0.9999	271.55	0.9999

used. This behavior confirms the complex mechanism of the glass-ceramics crystallization process, involving probably a self-accelerating effect. As a result, the calculated activation energies are apparent values, depending on the activation energy of the elementary processes (nucleation and growth) involved in the crystallization process. This behavior is similar to that of some glass-ceramics [20–23].

In order to obtain more information about the complex mechanism of the crystallization process, the Avrami exponent *n* was determined using Ozawa method (Eq. (7)).

The plots of log[–ln(1–α)] *vs.* logβ at different temperatures for sample GS2 are presented in Fig. 9.

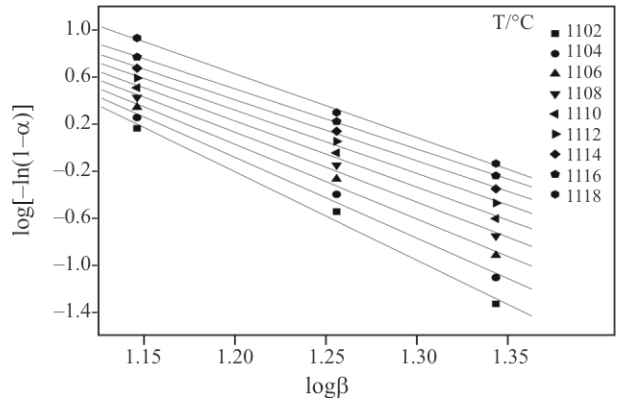

Fig. 9 Plots of log[–ln(1–α)] as a function of logβ for sample GS2 at different temperatures

Table 3 Avrami exponents *n* and the correlation coefficients r^2 at different temperatures for samples GS1 and GS2

GS1			GS2		
Temperature *T*/°C	*n*	r^2	Temperature *T*/°C	*n*	r^2
1126	6.24	0.9985	1094	7.97	0.9913
1128	6.03	0.9994	1096	7.56	0.9965
1130	5.86	0.9997	1098	7.91	0.9990
1132	5.73	0.9999	1100	7.13	0.9980
1134	5.63	0.9999	1102	7.57	0.9956
1136	5.57	0.9999	1104	6.90	0.9962
1138	5.58	0.9996	1106	6.39	0.9966
1140	6.12	0.9994	1108	5.98	0.9971
1148	7.86	0.9900	1110	5.66	0.9977
1150	7.73	0.9901	1112	5.41	0.9984
1152	7.17	0.9939	1114	5.23	0.9992
1154	6.85	0.9951	1116	5.14	0.9999
1156	6.64	0.9957	1118	5.46	0.9991

Table 3 summarizes the values of Avrami exponent calculated by using Ozawa method, for samples GS1 and GS2, at different temperatures ($1\%<\alpha<99\%$).

As it may be seen from the data presented in Table 3, for both samples, the Avrami exponent has values higher than four ($n>4.0$), varying from $n=5.14$ to 7.97.

These high values for n indicate that the studied crystallization mechanism of the silica gels cannot be described by the Johnson–Mehl–Avrami (JMA) model.

Regarding the crystallization kinetics, Weinberg *et al.* demonstrated [24, 25] the necessity of the JMA model extension, taking into account the finite size effect and non-uniform nucleation, the non-spherical, anisotropic particles formation during the crystallization process and the transient nucleation effect.

Conclusions

A surface area 100 times bigger does not determine significant changes in the activation energy of the silica gels crystallization process. Therefore, a 100 times decrease of the surface area (from $S=252.62$ m^2 g^{-1} in the case of GS2 sample to $S=2.52$ m^2 g^{-1} in the case of GS1 sample) only results in a slight activation energy increase.

The isoconversional analysis of the silica gels crystallization processes shows the dependence of the activation energy on the crystallized fraction which confirms that the crystallization mechanism is complex and the calculated activation energies are apparent values.

The Avrami exponent calculated with Ozawa method has high values varying from $n=5.14$ to 7.97 for both samples, indicating that the JMA model cannot be used for the crystallization of the studied silica gels.

References

1 W. Hinz, Silikate,VEB Verlag fur Bauwesen, Berlin 1971.
2 E. M. Levin, C. R. Robbins and H. F. McMurdie, Phase Diagrams for Ceramists, The American Ceramic Society, Ohio 1964.
3 M. J. Starink, J. Mater. Sci., 42 (2007) 483.
4 P. Simon, J. Therm. Anal. Cal., 76 (2004) 123.
5 J. M. Cai and R. H. Liu, J. Therm. Anal. Cal., 91 (2008) 275.
6 T. Ozawa, Bull. Chem. Soc. Jpn, 38 (1965) 1881.
7 C. D. Doyle, J. Appl. Polym. Sci., 6 (1962) 639.
8 M. J. Starink, Thermochim. Acta, 404 (2003) 163.
9 N. Sbirrazzuoli, L. Vincent, J. Bouillard and L. Elegant, J. Therm. Anal. Cal., 56 (1999) 783.
10 P. Murray and J. White, Trans. Brot. Ceram. Soc., 54 (1955) 204.
11 A. W. Coats and J. P. Redfern, Nature, 201 (1964) 68.
12 M. J. Starink, Thermochim. Acta, 288 (1996) 97.
13 T. Wanjun, L. Yuwen, Z. Hen and W. Cunxin, Thermochim. Acta, 408 (2003) 39.
14 T. Wanjun and C. Donghua, Thermochim. Acta, 433 (2005) 72.
15 M. Avrami, J. Chem. Phys., 9 (1941) 177.
16 J. Malek, J. Therm. Anal. Cal., 56 (1999) 763.
17 T. Ozawa, J. Thermal Anal., 2 (1970) 301.
18 T. Ozawa, Polymer, 12 (1971) 150.
19 T. Ozawa, J. Therm. Anal. Cal., 82 (2005) 687.
20 C. Păcurariu, M. Liţă, I. Lazău, D. Tiţa and G. Kovacs, J. Therm. Anal. Cal., 72 (2003) 811.
21 C. Păcurariu, D. Tiăa, R. I. Lazău, G. Kovacs and I. Lazău, J. Therm. Anal. Cal., 72 (2003) 823.
22 C. Păcurariu, R. I. Lazău, I. Lazău and D. Tiţa, J. Therm. Anal. Cal., 88 (2007) 3 647.
23 T. Vlase, C. Păcurariu, R. I. Lazău and I. Lazău, J. Therm. Anal. Cal., 88 (2007) 3 625.
24 M. C. Weinberg, D. P. Birnie III and V. A. Shneidman, J. Non-Cryst. Solids, 219 (1997) 89.
25 M. C. Weinberg, J. Non-Cryst. Solids, 255 (1999) 1.

ICTAC 2008

DOI: 10.1007/s10973-008-9680-0